Available online at www.sciencedirect.com
ScienceDirect
Trans. Nonferrous Met. Soc. China 26(2016) 1809−1819
Transactions of Nonferrous Metals Society of China
www.tnmsc.cn

Effects of sliding velocity and normal load on tribological behavior of aged Al−Sn−Cu alloy

Sheng-cheng ZHANG[1], Qing-lin PAN[1,2], Jie YAN[1], Xing HUANG[1]

1. School of Materials Science and Engineering, Central South University, Changsha 410083, China;
2. Nonferrous Metal Oriented Advanced Structural Materials and Manufacturing Cooperative Innovation Center, Central South University, Changsha 410083, China

Received 22 June 2015; accepted 13 October 2015

Abstract: The tribological behavior of aged Al−Sn−Cu alloy rubbed in the presence of lubricant over a range of sliding velocities and normal loads was investigated. The results showed that peak-aged (PA) alloy had a better tribological behavior than under-aged (UA) and over-aged (OA) alloys, which could be attributed to the optimized strength−ductility matching and a better hardness under PA condition. Wear rate and friction coefficient showed great sensitivity to applied sliding velocity and normal load. The wear rate and friction coefficient of the alloy exhibited a reduction trend with the increase in sliding velocity. The low wear rate and friction coefficient of alloy at high velocities were due to the effectively protected film and homogeneous Sn on surface. However, an increase in normal load led to an obvious increment in wear rate. The friction coefficient exhibited a fluctuant trend with the increase of normal loads. The seriously destroyed film and abraded Sn resulted in poor tribological behavior at high normal loads. The Sn particles and lubricant film which includes low shear interfacial lubricating layer and oxide tribolayer are the key to the tribological behavior of Al−Sn−Cu alloy.

Key words: Al−Sn−Cu alloy; tribological behavior; sliding velocity; normal load; aging

1 Introduction

Journal bearings are continuously demanded for better load-carrying capacity and wear resistance property with the development of modern machines to higher output and lower fuel consumption[1]. Al-based alloys containing Pb and Sn are widely used as bearing materials due to their fine load-carrying capacity, wear resistance and compatibility [2,3]. However, the lead-free bearing is the developing tendency of bearing materials due to the environmental health. Therefore, Al−Sn alloys are used in more and more applications as journal bearing materials [4]. With respect to conventional Al−Sn alloys, the further applications in machines are restricted. One of the possible reasons is the poor strength, which cannot satisfy the demand of high load in modern machines [5]. In addition, due to the immiscibility of Al−Sn system, the homogeneous distribution of Sn in Al matrix is not easy to achieve in conventional casting of Al−Sn alloy [6], which results in poor tribological behavior [3]. Considerable efforts have been made to overcome those drawbacks, such as stir cast [2], rapid solidification [7,8], physical vapor deposition [9], electrodeposition [10], severe plastic deformation [11], mechanical alloy [12], alloying addition [7,13,14] and intensive melt shearing [15]. Through optimization of alloying addition, the mechanical properties and wear behavior of alloy could be greatly improved. The addition of Cu has significant influences on microstructure and wear properties of Al−Pb alloys [16]. Similar information was also found by LU et al [17] and BANERJEE et al [18]. LU et al [17] observed the role of Mg addition in wear performance of dual-scale Al−Sn alloys and found that the appropriate addition of Mg could increase wetability and improve distribution of Sn phase, strength and ductility of alloy. BANERJEE et al [18] investigated the influence of Sn on the mechanical properties and age-hardening behavior of Al−Cu−Mg alloys and proved that the hardness and strength of alloy increase with the addition of Sn.

The tribological behavior of alloy is influenced by

Foundation item: Project (2013AH100055) supported by the Special Foundation for Science and Technology Innovation of Foshan, China
Corresponding author: Qing-lin PAN; Tel/Fax: +86-731-88830933; E-mail: pqlmte102@126.com
DOI: 10.1016/S1003-6326(16)64292-9

several factors, which include mechanical properties and wear conditions [19]. It is generally recognized that the tribological behavior of alloy has a close relationship with hardness and mechanical properties [20,21]. Previous results [22,23] showed that better mechanical properties of alloy are achievable by thermal aging treatment. Meanwhile, lots of studies have indicated that the tribological behavior has a significant correlation with sliding velocity and normal load [24,25]. As the two important parameters which significantly affect the wear behavior, the effects of load and sliding velocity on wear rate of Al−Si alloys are interdependent especially under severe sliding conditions [24]. The wear resistance of a nanocrystalline Al-based composite at high velocity and low load is improved and it is attributed to the increased tribolayer coverage on the worn surface [25]. It seems that the transfer layer determines the wear behavior of alloy at different sliding velocities and normal loads. An increase in normal load and sliding velocity creates an intermetallic wear-induced layer, which modifies the wear behavior of Cu−0.65%Cr (mass fraction) alloy [26]. The friction coefficient of copper was found to be correlated with the size and distribution of the transfer layer at different sliding velocities [27]. As is well known, the lubricant conditions determine the tribological performance of alloy. Unfortunately, the wear behavior of Al−Sn alloys was almost studied under unlubricated condition [3,5,17,21].

In this work, the hardness and strength of Al−Sn alloy have been improved by the addition of Cu. It was found that the hardness of alloy increased from HV 30 to HV 70 after the addition of Cu. Homogenization treatment and hot extrusion were carried out on Al−Sn−Cu alloy in order to improve the homogeneous distribution of Sn in Al matrix. The tribological behavior of the alloy was studied under lubricating condition which is close to the real applications [28]. The objective of the current work is two-fold: firstly, to observe the tribological performance of Al−Sn−Cu alloy under different aging treatment; secondly, to focus on exploring the effects of sliding velocity and normal load on tribological behavior of alloy under lubricating condition.

2 Experimental

The studied alloy was prepared by direct water-cooling casting and the nominal composition of the alloy is given in Table 1. To improve the homogeneous distribution of Sn in Al matrix, the Al−Sn−Cu alloy was homogenized at 480 °C for 19 h and then hot-extruded by 25 MN extruding machine at the extrusion temperature of 380 °C and extrusion ratio of 20. The samples were solution-treated in air atmosphere at 490 °C for 1 h and then quenched in cold water. Subsequently, all the samples were aged at 190 °C for 1, 2, 4, 6 and 12 h, respectively.

Table 1 Nominal composition of Al−Sn−Cu alloy (mass fraction, %)

Sn	Cu	Fe	Si	Zn	Al
3.61	3.48	0.09−0.10	0.06−0.07	0.02−0.03	Bal.

Hardness measurement was carried out on samples by a microvickers hardness testing machine at a load of 200 g. Tensile test was implemented on the MTS−810 type electrohydraulic servo-controlled material testing machine at a rate of 2 mm/min. The precipitates were observed by transmission electron microscopy (TEM) using a Tecnai $G^2$20S-TWIN transmission electron microscope. Friction and wear tests were performed on the UMT−3 wear tester in ambient environment for 30 min. The samples were machined into a cuboid with dimensions of 25 mm × 25 mm × 20 mm. The wear test was performed under lubricating condition which is close to the real applications and the lubrication was accomplished by using CD15W/40 diesel engine oil. The grinding ring has a size of *d*9.5 mm × 9.5 mm and hardness of HRC 62. The wear test was carried out at sliding speeds of 0.04, 0.08 and 0.12 m/s, respectively, under normal loads of 50, 100 and 150 N.

The samples were polished, and then ultrasonically cleaned in absolute ethanol and dried before wear test. The friction coefficient varying with the sliding duration was continuously recorded by a computer connected with the wear tester. The wear volume (ΔV) was calculated as the following relationship [29]:

$$\Delta V = B\left[\pi\frac{r^2}{180}\sin^{-1}\left(\frac{b}{2r}\right)-\frac{b}{2\sqrt{\left(r^2-\frac{b^2}{4}\right)}}\right] \quad (1)$$

In the present study, the wear volume was simplified from Eq. (1) and characterized by

$$\Delta V = \frac{Bb^3}{12r} \quad (2)$$

where B is the length of the wear track, r is the radius of the grinding ring, b is the width of the wear track. Wear rate was calculated by dividing the wear volume by sliding distance (30 min × (0.04−0.12) m/s). The worn morphology and microstructure were observed by scanning electron microscopy (SEM) using a FEI Quanta−200 scanning electron microscope. Moreover, cross-sectional samples perpendicular to the worn surface were cut, ground and polished for SEM

observation of the subsurface microstructure.

3 Results

3.1 Effect of aging treatment on tribological behavior of Al−Sn−Cu alloy

Figure 1 shows the variation of Vickers hardness and mechanical properties of Al−Sn−Cu alloy as a function of aging time at 190 °C. It is obvious that aging at 190 °C increases hardness with time until it reaches a peak after 4 h, and then the hardness decreases as time elapses. The ultimate tensile strength R_m and yield strength R_p increase as the aging time extends, but they begin to decrease when reaching the peak at 4 h, which is similar to the variation of hardness. However, the elongation A decreases as aging time elapses. As is well known, the θ' phase plays an important role in strengthening of Al−Cu−Sn alloys. During the age hardening treatment, θ' phase precipitates uniformly in matrix, thereby increasing the strength of these alloys [30]. Bright field TEM images are shown in Fig. 2 for the under-aged (UA, 1 h), peak-aged (PA, 4 h) and over-aged (OA, 12 h) conditions. For the UA condition, plate-shaped θ' phase is not observed. However, the significant plate-shaped θ' phase is observed under the PA condition, as expected. Its size is relatively uniform and distribution is homogeneous. Under the OA condition, the θ' phase has grown up and coarsened. The mobility of dislocations is impeded by second-phase particles in two distinct ways, it may either cut the second-phase particles or bypass them. At the early stage of aging, the hardness and strength of alloy are the lowest because θ' phase has not formed and the mobility of dislocations is not retarded. Under the PA condition, the θ' phase is very fine and uniform, and dislocations cut and deform the particles, leading to the highest hardness and strength. On the other hand, the growth of θ' phase under OA condition causes the increase of the interparticle spacing. Large interparticle spacing between precipitates weakens their role due to retarding the mobility of dislocation, thus contributing to a decrease in hardness and strength.

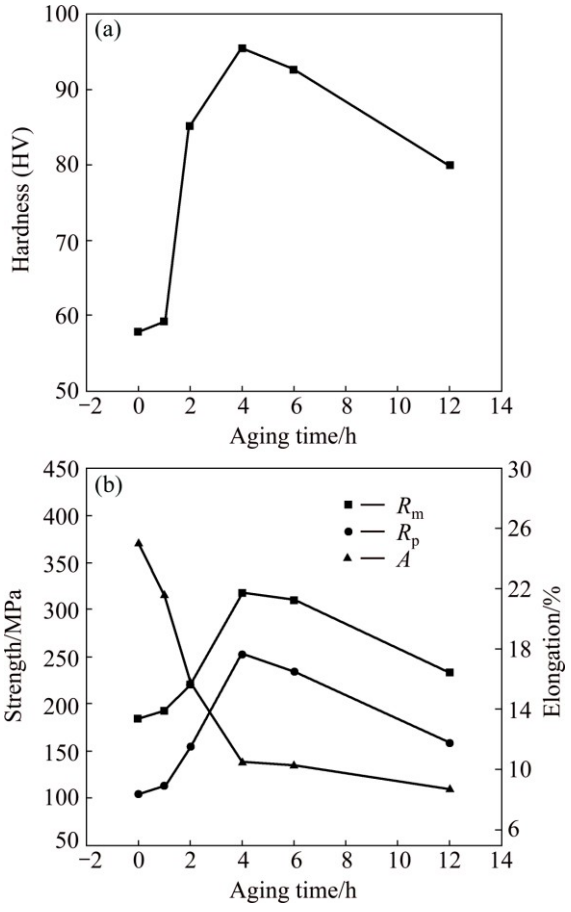

Fig. 1 Hardness (a) and mechanical properties (b) of Al−Sn−Cu alloy as function of aging time at 190 °C

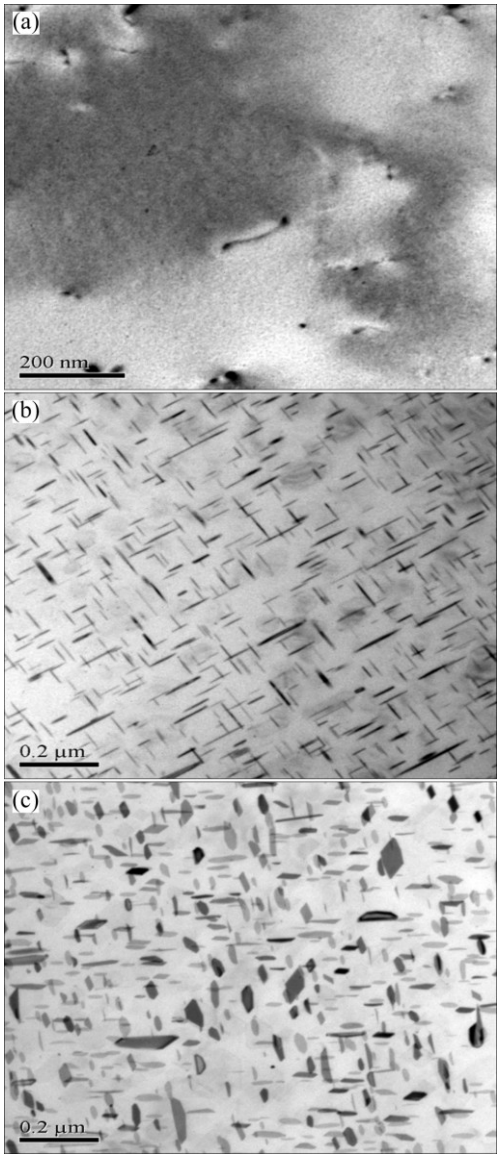

Fig. 2 Bright field TEM images showing microstructure after 1 h (UA) (a), 4 h (PA) (b) and 12 h (OA) (c) at 190 °C

Figure 3 shows the variation of wear rate and friction coefficient of the alloy under UA, PA and OA conditions as a function of sliding velocity at a normal load of 100 N. It is obvious that the wear rate and friction coefficient exhibit a reduction and then an incremental trend with the increase in aging time. The lowest wear rate and friction coefficient occur under PA condition. This demonstrates that the alloy under PA condition has much better anti-friction behavior and load-carrying capacity than that under UA and OA conditions. The difference in wear properties mentioned above can be further revealed by observing the worn surface morphologies of the alloy under UA, PA and OA conditions at a sliding speed of 0.08 m/s and a normal load of 100 N, as shown in Fig. 4. It is interesting to find that there exist plow grooves on the worn surface under all conditions. Nevertheless, there are numerous cracks on the worn surface shown in Figs. 4(a) and (c), which mainly be parallel to the sliding direction. Furthermore, the adhesion traces are observed in Fig. 4(a). The above observation on worn surface suggests that the surface under PA condition is the best, which can further prove that the alloy under PA condition has a better tribological behavior.

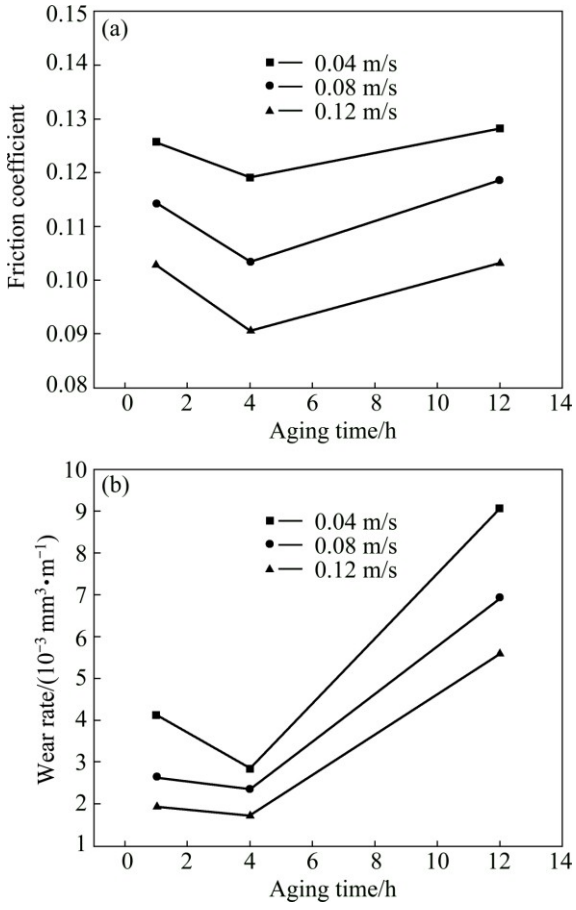

Fig. 3 Variation of friction coefficient (a) and wear rate (b) of alloy under UA, PA and OA conditions as function of sliding velocity at nominal load of 100 N

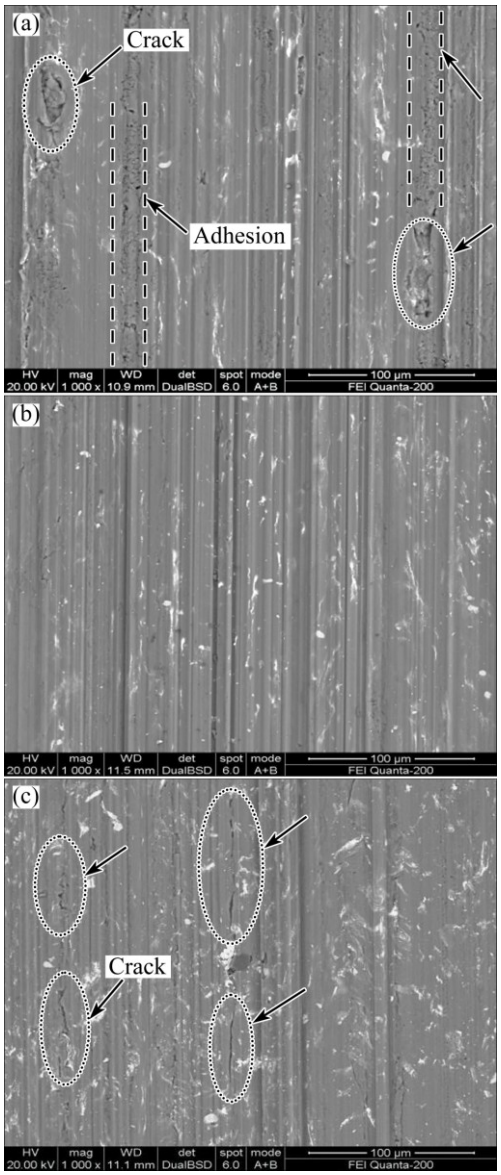

Fig. 4 Worn surface morphologies of alloy under UA (a), PA (b) and OA (c) conditions at sliding speed of 0.08 m/s and normal load of 100 N

The tribological behavior of the alloy has a close relationship with hardness and mechanical properties. It is generally recognized that hardness is one of the key factors which influence the sliding behavior of different alloys [20]. Hardness value of the material is inversely proportional to wear rate, so that hard alloys have greater wear resistances [31]. FEYZULLAHOGLU and SAKIROGLU [32], RAMESH and SAFIULLA [33] noticed that the improved hardness causes the decrease of wear rate. However, the fine tribological behavior is the result of excellent strength−ductility matching. The low ductility of alloy limits further improvement of its wear resistance [21]. The optimized combination of hardness and toughness is a key for the improvement of wear properties [34]. Similar results were presented in the studies [35,36]. Under the PA condition, the alloy has

an optimized strength−ductility matching and a better hardness (Fig. 1), which leads to the fine wear performance (Figs. 3 and 4).

It is clear that the alloy achieves the fine tribological performance under PA condition. Therefore, an alloy under this aging condition was chosen for exploring the effect of sliding velocity and normal load on tribological behavior.

3.2 Effects of sliding velocity and normal load on tribological behavior of peak-aged Al−Sn−Cu alloy

The wear rate of peak-aged Al−Sn−Cu alloy with the variation of sliding velocity and normal load is presented in Fig. 5. It can be seen that the wear rate decreases with the increase of sliding velocity under all normal load conditions. It is worthy to note that the wear rate drops down from 13.9×10^{-3} to 3.5×10^{-3} mm^3/m when the sliding velocity varies from 0.04 to 0.08 m/s at the normal load of 150 N. However, the wear rate increases with the increase in normal load, especially at low sliding velocity. The highest wear rate occurs at the sliding speed of 0.04 m/s and normal load of 150 N, which could be attributed to the severely abraded surface resulted from damaged film.

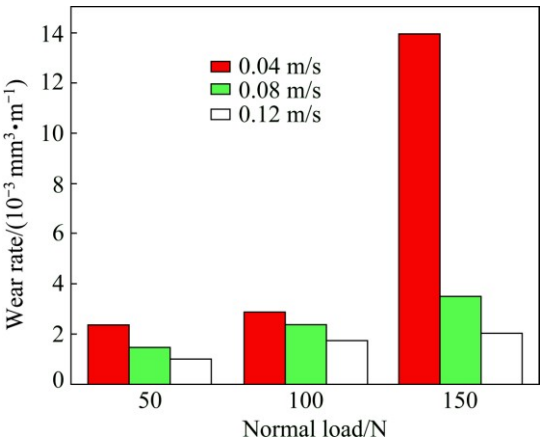

Fig. 5 Variation of wear rate of peak-aged Al−Sn−Cu alloy as function of normal load and sliding velocity

In order to reveal the results observed above in more detail, SEM analysis was carried out on the worn surface of samples. Figure 6 shows the morphologies of worn surface at various sliding velocities and normal loads. It is apparent from Fig. 6(g) that the worn surface is damaged seriously at the sliding velocity of 0.04 m/s and normal load of 150 N, which is in accordance with the highest wear rate. There are visible cracks, adhesions and plow grooves on the worn surfaces at low sliding velocities, in particular, the cracks and adhesions are more obvious and severer with the increase of normal load. At a sliding velocity of 0.12 m/s and a normal load of 50 N, the worn surface is smooth, as shown in Fig. 6(c). It seems that the surface is smoother at higher sliding velocities, while that at lower velocities is rough and presents evident cracks and adhesions.

Figure 7 shows the variation of the average steady-state coefficient of friction as a function of sliding velocity and normal load. As can be seen that at a constant load, an increase in sliding velocity leads to a decrease in friction coefficient, which may be due to the increasing film and the uniform distribution of dispersed Sn on the surface. The friction coefficient exhibits a fluctuant trend with the increase in normal load. Friction coefficient decreases slightly with the increase in normal load and a low sliding velocity of 0.04 m/s. The possible reason is that the increase in contact load tends to enlarge the real contact area and to reduce contact pressure, hence reducing the friction coefficient. However, it is noticed that the alloy exhibits a reduction, and then incremental trend in friction coefficient with the increase in normal load at sliding velocities of 0.08 and 0.12 m/s. An increase in friction coefficient at sliding velocities of 0.08 and 0.12 m/s and the normal load higher than 100 N can be attributed to the abraded Sn on the surface and damaged film under such conditions.

3.3 Analysis of lubricant film

The tribological behavior of Al−Sn−Cu alloy was studied under lubricating condition. The Stribeck curve plays an important role in identifying different lubricant regimes [37]: elastohydrodynamic lubrication (EHL), mixed lubrication (ML) and boundary lubrication (BL). The EHL regime is accompanied at low loads and high sliding velocities, the low values of friction coefficient and wear rate are obtained in this regime. However, the high loads and low sliding velocities indicate BL regime which has high values of friction coefficient and wear rate. Actually, BL regime is closer to the real applications where continuous lubricating is nearly impossible. According to the Stribeck curve for steel pin tested against steel disc and Al−Si P/M disc given by TIMMERMANS and FROYEN [38], the friction coefficient is 0.08−0.12 in BL regime while in EHL regime it is below 0.02. The above results of friction coefficient shown in Fig. 7 indicate the BL regime. Adhesion and plow groove are the major characteristics in BL regime which has been described by MESHI et al [39], MOSHKOVICH et al [40] and PERFILYEV et al [41]. It is apparent from Fig. 6 that adhesion and plow groove exist almost on the all worn surfaces, which further proves the BL regime.

The tribological behavior of Al−Sn−Cu alloy is strongly dependent upon the formation of a thin lubricant film between the two mating surfaces and the lubrication

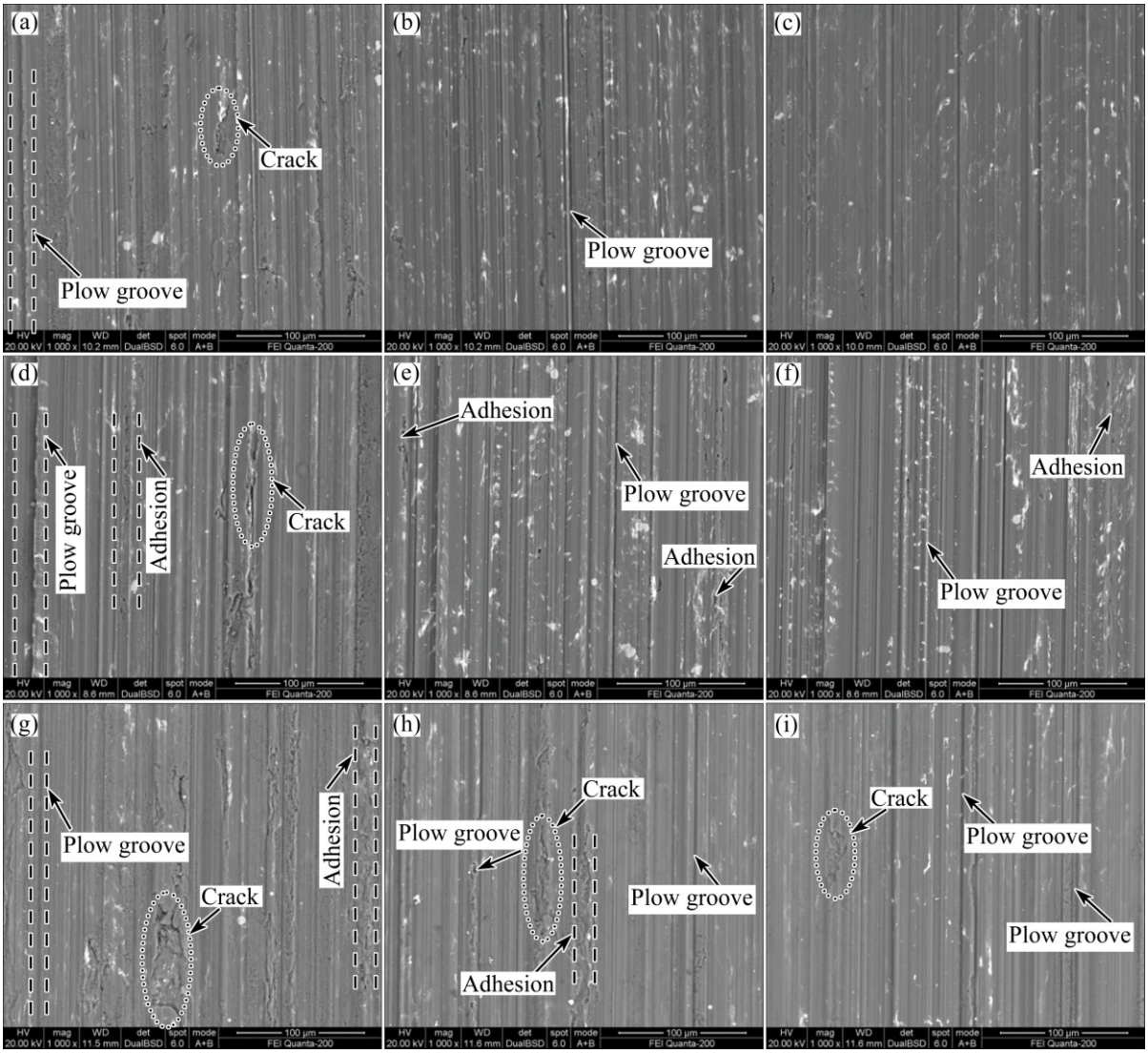

Fig. 6 SEM images of worn surface at different sliding velocities and normal loads: (a) 50 N, 0.04 m/s; (b) 50 N, 0.08 m/s; (c) 50 N, 0.12 m/s; (d) 100 N, 0.04 m/s; (e) 100 N, 0.08 m/s; (f) 100 N, 0.12 m/s; (g) 150 N, 0.04 m/s; (h) 150 N, 0.08 m/s; (i) 150 N, 0.12 m/s

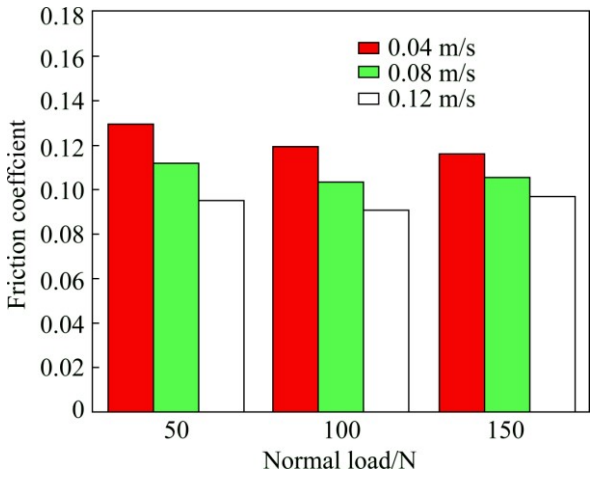

Fig. 7 Variation of friction coefficient with normal load and sliding velocity of peak-aged Al−Sn−Cu alloy

performance of Sn particles in BL regime. Compositionally, BL film can be regard as a compound film composed of both a hard load supporting layer and a soft, easily shearable layer [42]. The BL film is influenced by several mechanisms combined. Possible mechanisms and function factors include low shear interfacial lubricating layer, friction modifying layer, load-bearing solids, shear resistant layer, and sacrificial layer [43]. Under the studied conditions, the dominant factors of BL film are low shear interfacial lubricating layer and friction modifying layer (oxide tribolayer). The low shear interfacial lubricating layer is similar to the film for the steady-state smooth-surface EHL contact [40], whose thickness h_c could be expressed by a simple power law of the form [44]:

$$\overline{H}_c = k\overline{U}^a\overline{G}^b\overline{W}^c f\left(R'_y / R'_x\right) \quad (3)$$

where $\overline{H}_c = h_c / R'_x$ is the film thickness parameter, $\overline{U} = U\eta_0 / (E'R'_x)$ is the speed parameter, $\overline{G} = \alpha E'$ is the material parameter, $\overline{W} = W / (E'R'^2_x)$ is the load parameter, and $f(R'_y / R'_x)$ is a function describing the influence of contact ellipticity on the film thickness, a, b and c are constants having typical values of approximately a = 0.7, b = 0.5, and c =−0.1. According to Eq. (3), the low shear interfacial lubricating layer is dependent on all three parameters. Furthermore, the thickness of interfacial lubricating layer is clearly proportional to sliding velocity, while it is inversely proportional to normal load. At high normal loads and low sliding velocities, low shear interfacial lubricating layer is very thin and almost breaks down, which results in the direct contact of two mating surfaces and the high wear rate (Fig. 5), showing poor wear behavior. However, the low shear interfacial lubricating layer is relatively effectively protected at low normal loads and high sliding velocities. The interfacial lubricating layer is good and the mating surfaces are detached, leading to a low wear rate and a fine tribological behavior.

Another dominant factor of BL film is friction modifying layer (oxide tribolayer). Since oxide tribolayer plays an important role in the tribological behavior [45], any factors changing the formation of tribolayer will influence the wear performance of the alloy. Figure 8 shows the SEM images showing the cross-sectional morphologies of worn subsurface as a function of sliding velocity at a normal load of 50 N. It is interesting to find that the thickness of tribolayer decreases with the increase in sliding velocity at a normal load of 50 N. According to the above analysis, the thickness of interfacial lubricating layer is clearly proportional to sliding velocity. It is quite natural that the thickness of interfacial lubricating layer at high sliding velocities is higher than that at low sliding velocities. As is well known, lubricating layer not only separates the two mating surfaces, but also cools the contact surfaces. The thick lubricating layer could sufficiently decreases the temperature of surfaces, resulting in the lower temperature at high sliding velocities. With an increase in sliding velocity, oxide formation is restrained due to the decreasing temperature [26], which leads to the thin oxide tribolayer at high sliding velocities. However, the low shear interfacial lubricating layer is effectively protected at low normal loads and the effect of interfacial lubricating layer is more dominant than that of oxide tribolayer under this condition. Therefore, due to the thick interfacial lubricating layer at high sliding velocities, the wear rate decreases with the increase in sliding velocity (Fig. 5) despite the thin tribolayer at high sliding velocities. The severe damage on the thick tribolayer shown in Fig. 9(a) apparently proves the poor tribological behavior at a low sliding velocity.

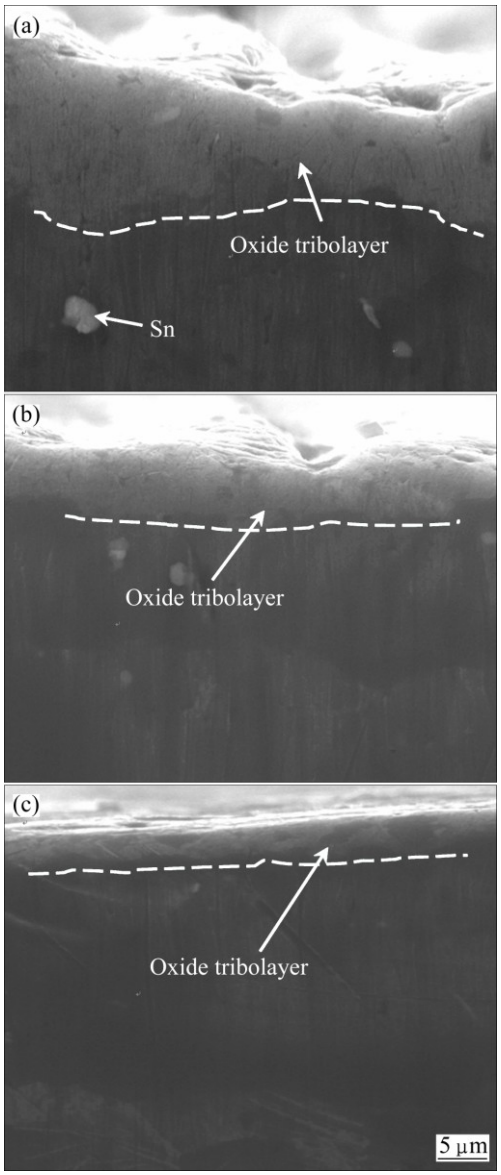

Fig. 8 SEM images showing cross-sectional morphologies of worn subsurface at normal load of 50 N and different sliding velocities: (a) 0.04 m/s; (b) 0.08 m/s; (c) 0.12 m/s

Figure 9 shows the SEM images for cross-sectional morphologies of worn subsurface as a function of sliding velocity at a normal load of 150 N. It is apparent that the damage of tribolayer is more and more serious with the decrease of sliding velocity. The effect of oxide tribolayer is more dominant than that of interfacial lubricating layer at high normal load. This is because there are much higher pressure and temperature which promote the formation of oxide tribolayer and the interfacial lubricating layer is almost broken down at high normal loads. It can be seen that the tribolayer is smooth at a sliding velocity higher than 0.08 m/s. Both the smooth tribolayer and relatively thick interfacial lubricating layer may lead to an abrupt drop in wear rate at higher sliding velocity of 0.08 m/s and normal load of 150 N, as shown in Fig. 5. It can be seen from Figs. 8

and 9 that the tribolayer is damaged seriously at high normal loads, while it is continuous at low normal loads. The damage of tribolayer can be attributed to the severe plastic deformation on subsurface layers, which can be proved by the strip-shaped Sn particles in Fig. 9(b) compared with the globular Sn in Fig. 8(a). The seriously destroyed tribolayer results in poor tribological behavior at high normal loads.

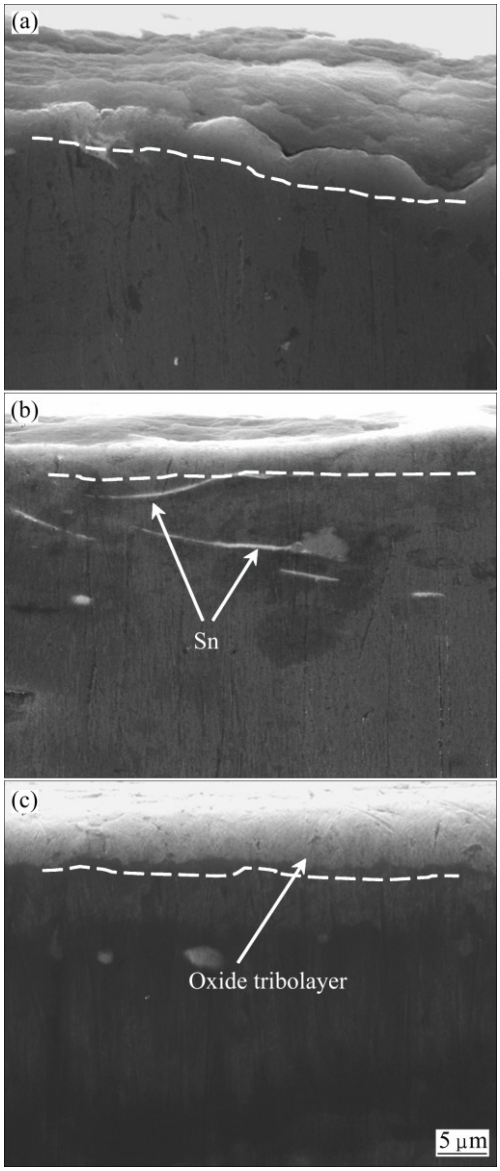

Fig. 9 SEM images showing cross-sectional morphologies of worn subsurface at normal load of 150 N and different sliding velocities: (a) 0.04 m/s; (b) 0.08 m/s; (c) 0.12 m/s

3.4 Analysis of Sn particles

Al−Sn alloy is suitable for sliding bearing applications owing to its fine tribological property and the Sn phase plays an important role in the tribological behavior of the alloy [3,17]. During sliding, the Sn phase is smeared out on the surface and protects the surface serving as solid lubricant. Solid lubricants in self-lubricating materials seem to be more promising than liquid lubricants, particularly at high temperatures, in vacuum environments, and in sealed systems [46]. In general, continuous and homogeneous distribution of Sn which serves as solid lubricant is beneficial to tribological behavior.

Different distributions of Sn particles on the worn surface are presented in Figs. 10 and 11. The light grey phase *A* shown in Fig. 10(a) is Sn, which can be proved by the EDS analysis in Fig. 10(c). It is obvious that the Sn particles are continuous and homogeneous at high sliding velocities and low normal loads, while the Sn particles almost completely disappear at low sliding velocities and high normal loads, as shown in Fig. 10. Sn effectively separates the two mating surfaces and protects the surface of samples from being damaged. The

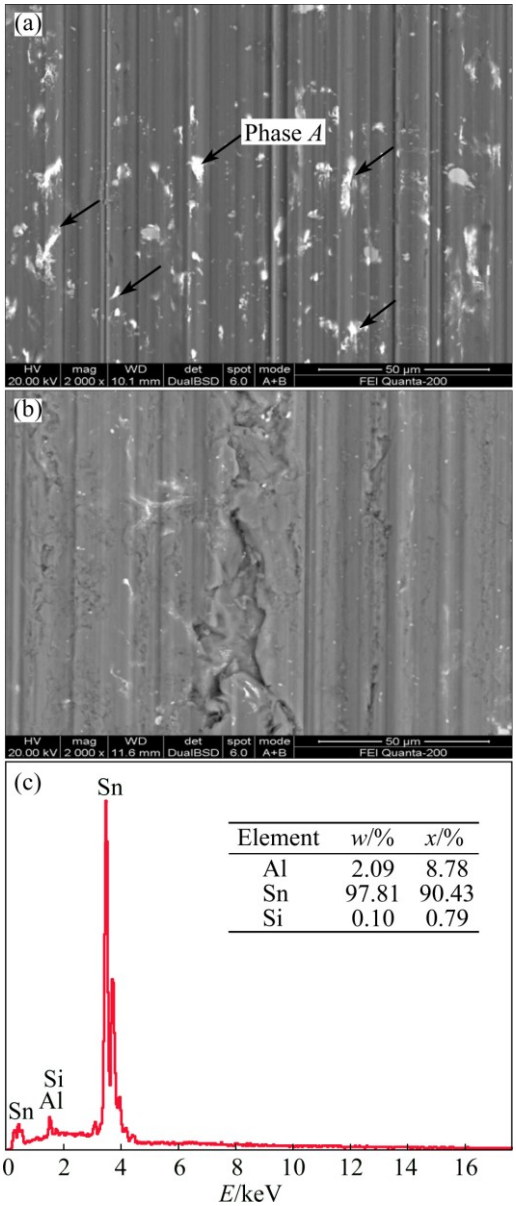

Fig. 10 SEM images of worn surfaces at sliding velocity of 0.12 m/s and normal load of 50 N (a), sliding velocity of 0.04 m/s and normal load of 150 N (b) and EDS analysis of phase *A* (c)

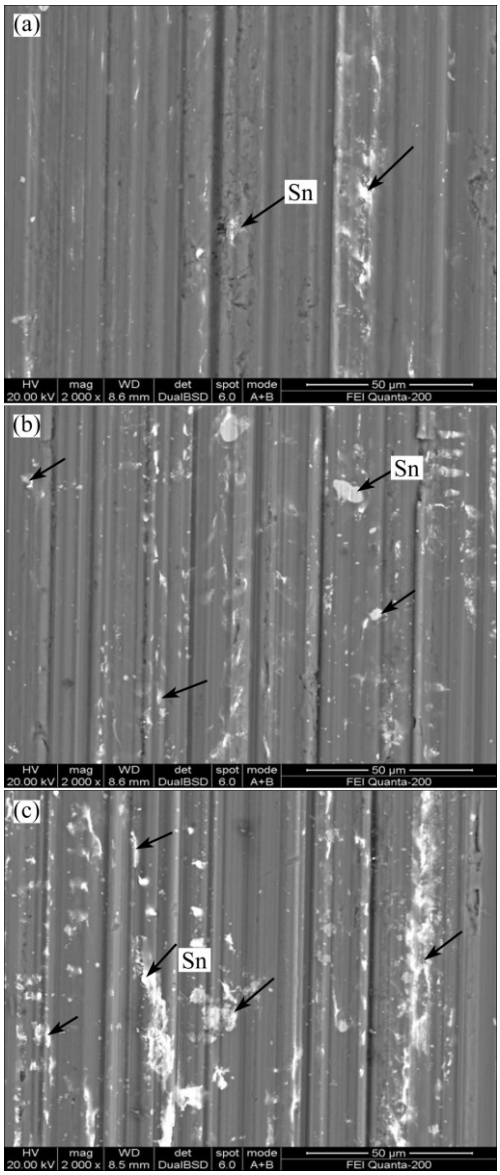

Fig. 11 SEM images of worn surfaces showing variation of Sn phase (light grey) as function of sliding velocity at normal load of 100 N and different sliding velocities: (a) 0.04 m/s; (b) 0.08 m/s; (c) 0.12 m/s

difference in wear rate and friction coefficient between high sliding velocity, low normal load and low sliding velocity, high normal load conditions shown in Figs. 5 and 7 is in good agreement with the huge different distribution of Sn on surface. Figure 11 shows the variation of distribution of Sn particles as a function of sliding velocity at a normal load of 100 N. It can be seen that the Sn particles are more continuous and homogeneous with the increase in sliding velocity, which can well explain the decreasing friction coefficient and wear rate with the increase in sliding velocity. To a great extent, the reduction of friction coefficient and wear rate is attributed to the more and more continuous and homogeneous Sn particles on the surface.

4 Conclusions

1) The tribological behavior of Al−Sn−Cu alloy has a close relationship with hardness and mechanical properties. With increasing in aging time, the wear rate and friction coefficient of the alloy tend to decline firstly and then increase. The PA alloy achieves the fine tribological performance due to the optimized strength−ductility matching and a better hardness.

2) The tribological behavior of Al−Sn−Cu alloy is dependent on sliding velocity and normal load. The wear rate of the alloy decreases with the increase of sliding velocity, while it exhibits an incremental trend with the increase in normal load. The friction coefficient decreases with the increase of sliding velocity under all normal load conditions. However, it exhibits a fluctuant trend with the increase in normal load. The friction coefficient decreases slightly with the increase in normal load at a low sliding velocity of 0.04 m/s, while it exhibits a reduction first and then an incremental trend with the increase in normal loads at sliding velocities of 0.08 and 0.12 m/s.

3) The tribological behavior of Al−Sn−Cu alloy is determined by the Sn particles on surface and lubricant film which includes low shear interfacial lubricating layer and oxide tribolayer under studied conditions. The lubricant film is effectively protected and the Sn particles are continuous and homogeneous at high sliding velocities and low normal loads, which leads to the fine tribological behavior of the alloy. However, the severely damaged lubricant film and Sn particles at low sliding velocities and high normal loads tend to result in poor tribological behavior.

References

[1] ÜNLÜ B S, DURMUS H, AKGÜN S. Tribological and mechanical properties of Al alloyed bearings [J]. Journal of Alloys and Compounds, 2009, 487: 225−230.

[2] PATHAK J P, MOHAN S. Tribological behaviour of conventional Al−Sn and equivalent Al−Pb alloys under lubrication [J]. Bulletin of Materials Science, 2003, 263: 15−320.

[3] LIU X, ZENG M Q, MA Y, ZHU M. Wear behavior of Al−Sn alloys with different distribution of Sn dispersoids manipulated by mechanical alloying and sintering [J]. Wear, 2008, 265: 1857−1863.

[4] BRAVO A E, DURAN H A, JACOBO V H, ORTIZ A, SCHOUWENAARS R. Towards new formulations for journal bearing alloys [J]. Wear, 2013, 302: 1528−1535.

[5] LIU X, ZENG M Q, MA Y, ZHU M. Promoting the high load-carrying capability of Al−20wt%Sn bearing alloys through creating nanocomposite structure by mechanical alloying [J]. Wear, 2012, 294−295: 387−394.

[6] KOTADIA H R, DAS A, DOERNBERG E, SCHMID-FETZER R. A comparative study of ternary Al−Sn−Cu immiscible alloys prepared by conventional casting and casting under high-intensity ultrasonic irradiation [J]. Materials Chemistry and Physics, 2011, 131: 241−249.

[7] YAN N, HONG Z Y, GENG D L, WANG W L, WEI B. Phase separation and structure evolution of ternary Al−Cu−Sn immiscible alloy under ultrasonic levitation condition [J]. Journal of Alloys and Compounds, 2012, 544: 6−12.

[8] PRAMANICK A, CHATTERJEE S, BHATTACHARYA V, CHATTOPADHYAY K. Synthesis and microstructure of laser surface alloyed Al−Sn−Si layer on commercial aluminum substrate [J]. Journal of Materials Research, 2005, 20: 1580−1589.

[9] PERRONE A, ZOCCO A, ROSA H D, ZIMMERMANN R, BERSANI M. Al−Sn thin films deposited by pulsed laser ablation [J]. Materials Science and Engineering C, 2002, 22: 465−468.

[10] UEDA M, INABA R, OHTSUKA T. Composition and structure of Al−Sn alloys formed by constant potential electrolysis in an $AlCl_3$−NaCl−KCl−$SnCl_2$ molten salt [J]. Electrochimica Acta, 2013, 100: 281−284.

[11] NOSKOVA N I, VIL'DANOVA N F, FILIPPOV Y I, CHURBAEV R V, PERETURINA I A, KORSHUNOV L G, KORZNIKOV A V. Preparation, deformation, and failure of functional Al−Sn and Al−Sn−Pb nanocrystalline alloys [J]. Physics of Metals and Metallography, 2006, 102: 646−651.

[12] PATEL J, MORSI K. Effect of mechanical alloying on the microstructure and properties of Al−Sn−Mg alloy [J]. Journal of Alloys and Compounds, 2012, 540: 100−106.

[13] KONG C J, BROWN P D, HARRIS S J, MCCARTNEY D G. The microstructures of a thermally sprayed and heat treated Al−20wt.%Sn−3wt.%Si alloy [J]. Materials Science and Engineering A, 2005, 403: 205−214.

[14] WU Xiao-feng, ZHANG Guang-an, WU Fu-fa. Influence of Bi addition on microstructure and dry sliding wear behaviors of cast $AlMg_2Si$ metal matrix composite [J]. Transactions of Nonferrous Metals Society of China, 2013, 23: 1532−1542.

[15] KOTADIA H R, DOERNBERG E, PATEL J B, FAN Z, SCHMID-FETZER R. Solidification of Al−Sn−Cu based immiscible alloys under intense shearing [J]. Metallurgical and Materials Transactions A, 2009, 40: 2202−2211.

[16] ZHU M, ZENG M Q, GAO Y, OUYANG L Z, LI B L. Microstructure and wear properties of Al−Pb−Cu alloys prepared by mechanical alloying [J]. Wear, 2002, 253: 832−838.

[17] LU Z C, GAO Y, ZENG M Q, ZHU M. Improving wear performance of dual-scale Al−Sn alloys: The role of Mg addition in enhancing Sn distribution and tribolayer stability [J]. Wear, 2014, 309: 216−225.

[18] BANERJEE S J, ROBI P A, SRINIVASAN A, LAKAVATH P K. Effect of trace additions of Sn on microstructure and mechanical properties of Al−Cu−Mg alloys [J]. Materials and Design, 2010, 31: 4007−4015.

[19] PRABHU T R. Effects of solid lubricants, load, and sliding speed on the tribological behavior of silica reinforced composites using design of experiments [J]. Materials and Design, 2015, 77: 149−160.

[20] ZHANG Xiao-yu, REN Ping-di, ZHONG Fa-chun, ZHU Min-hao, ZHOU Zhong-rong. Fretting wear and friction oxidation behavior of 0Cr20Ni32AlTi alloy at high temperature [J]. Transactions of Nonferrous Metals Society of China, 2012, 22: 825−830.

[21] LU Z C, ZENG M Q, GAO Y, ZHU M. Significant improvement of wear properties by creating micro/nano dual-scale structure in Al−Sn alloys [J]. Wear, 2012, 296: 469−478.

[22] GOODARZY M H, ARABI H, BOUTORABI M A, SEYEDEIN S H, HASANI NAJAFABADI S H. The effects of room temperature ECAP and subsequent aging on mechanical properties of 2024 Al alloy [J]. Journal of Alloys and Compounds, 2014, 585: 753−759.

[23] HASSAN S B, AIGBODION V S. The effect of thermal ageing on microstructure and mechanical properties of Al−Si−Fe/Mg alloys [J]. Journal of Alloys and Compounds, 2009, 486: 309−314.

[24] DWIVEDI D K. Adhesive wear behaviour of cast aluminium–silicon alloys: Overview [J]. Materials and Design, 2010, 31: 2517−2531.

[25] LIU Y Q, HAN Z, CONG H T. Effects of sliding velocity and normal load on the tribological behavior of a nanocrystalline Al based composite [J]. Wear, 2010, 268: 976−983.

[26] ASADIKOUHANJANI S, ZAREBIDAKI A, AKBARI A. The effect of sliding speed and amount of loading on friction and wear behavior of Cu−0.65wt.%Cr alloy [J]. Journal of Alloys and Compounds, 2009, 486: 319−324.

[27] EMGEA A, KARTHIKEYANB S, KIMA H J, RIGNEY D A. The effect of sliding velocity on the tribological behavior of copper [J]. Wear, 2007, 263: 614−618.

[28] FEYZULLAHOöLU E, ERTÜRK A T, GÜVEN E A. Influence of forging and heat treatment on wear properties of Al−Si and Al−Pb bearing alloys in oil lubricated conditions [J]. Transactions of Nonferrous Metals Society of China, 2013, 23: 3575−3583.

[29] LI F, HU K, LI J, ZHAO B. The friction and wear characteristics of nanometer ZnO filled polytetrafluoroethylene [J]. Wear, 2002, 249: 877−882.

[30] BOURGEOIS L, DWYER C, WEYLAND M, NIE J F, MUDDLE B C. The magic thicknesses of θ' precipitates in Sn-microalloyed Al−Cu [J]. Acta Materialia, 2012, 60: 633−644.

[31] ALIDOKHT S A, ABDOLLAH-ZADEH A, SOLEYMANI S, SAEID T, ASSADI H. Evaluation of microstructure and wear behavior of friction stir processed cast aluminum alloy [J]. Materials Characterization, 2012, 63: 90−97.

[32] FEYZULLAHOGLU E, SAKIROGLU N. The tribological behaviours of aluminium-based materials under dry sliding [J]. Industrial Lubrication and Tribology, 2011, 63: 350−358.

[33] RAMESH C S, SAFIULLA M. Wear behavior of hot extruded Al6061 based composites [J]. Wear, 2007, 263: 620−635.

[34] LU Z C, ZENG M Q, GAO Y, ZHU M. Minimizing tribolayer damage by strength–ductility matching in dual-scale structured Al−Sn alloys: A mechanism for improving wear performance [J]. Wear, 2013, 304: 162−172.

[35] KUCUKOMEROGLU T. Effect of equal-channel angular extrusion on mechanical and wear properties of eutectic Al−12Si alloy [J]. Materials and Design, 2010, 31: 782−789.

[36] GAO N, WANG C T, WOOD R J K, LANGDON T G. Tribological properties of ultrafine-grained materials processed by severe plastic deformation [J]. Journal of Materials Science, 2012, 47: 4779−4797.

[37] LU X B, KHONSARI M M. The Stribeck curve: Experimental results and theoretical prediction [J]. Journal of Tribology, 2006, 128: 789−794.

[38] TIMMERMANS G, FROYEN L. Tribological performance of hypereutectic P/M Al−Si during sliding in oil [J]. Wear, 1999, 231: 77−88.

[39] MESHI L, SAMUHA S, COHEN S R, LAIKHTMAN A, MOSHKOVICH A, PERFILYEV V, LAPSKER I, RAPOPORT L. Dislocation structure and hardness of surface layers under friction of copper in different lubricant conditions [J]. Acta Materialia, 2011, 59: 342−348.

[40] MOSHKOVICH A, PERFILYEV V, GORNI D, LAPSKER I, RAPOPORT L. The effect of Cu grain size on transition from EHL to BL regime (Stribeck curve) [J]. Wear, 2011, 271: 1726−1732.

[41] PERFILYEV V, MOSHKOVICH A, LAPSKER I, RAPOPORT L. Friction and wear of copper samples in the steady friction state [J]. Tribology International, 2010, 43: 1449−1456.

[42] HSU S M, GATES R S. Boundary lubricating films: Formation and lubrication mechanism [J]. Tribology International, 2005, 38: 305−312.

[43] GLOVNEA R P, OLVER A V, SPIKES H A. Experimental investigation of the effect of speed and load on film thickness in elastohydrodynamic contact [J]. Tribology Transactions, 2005, 48: 328−335.

[44] GOHAR R. Elastohydrodynamics [M]. 2nd ed. London: Imperial College Press, 2002.
[45] SCHOUWENAARS R, JACOBO V H, ORTIZ A. Microstructural aspects of wear in soft tribological alloys [J]. Wear, 2007, 263: 727−735.
[46] LIN J F, SHIH M G, CHEN Y W. The tribological performance of 6061 aluminum alloy/graphite composite materials in oil lubrications with EP additives [J]. Wear, 1996, 198: 58−70.

摩擦速度和加载载荷对时效态 Al−Sn−Cu 合金摩擦磨损性能的影响

章升程[1]，潘清林[1,2]，严 杰[1]，黄 星[1]

1. 中南大学 材料科学与工程学院，长沙 410083；
2. 中南大学 有色金属先进结构材料与制造协同创新中心，长沙 410083

摘 要：研究在油润滑状态下摩擦速度和加载载荷对时效态 Al−Sn−Cu 合金摩擦磨损性能的影响。结果表明：由于峰时效合金较欠时效和过时效合金具有最佳的强度−塑性配比和更高的硬度，因此峰时效合金表现出最优的摩擦磨损性能。摩擦速度和加载载荷对合金磨损率和摩擦因数具有显著影响。随着摩擦速度的增大，磨损表面的润滑膜和 Sn 相更为均匀，合金的磨损率和摩擦因数均降低；然而随着加载载荷的增加，均匀的润滑膜和 Sn 相被严重破坏，合金磨损率急剧上升。Sn 相和包括中间润滑层、摩擦氧化层的润滑膜是影响 Al−Sn−Cu 合金摩擦磨损性能的决定性因素。

关键词：Al−Sn−Cu 合金；摩擦磨损性能；摩擦速度；加载载荷；时效

(Edited by Wei-ping CHEN)